water solubility, and it remained same HO inhibitory activity compared to native ZnPP. However, the loading of ZnPP in SMA–ZnPP micelle was much higher than that in PEG–ZnPP, which may substantially decrease the net weight of the compounds used for tumor therapy, thus reducing the viscosity of the injection solution and improve the therapeutic effectiveness/cost. Furthermore, from SMA–ZnPP micelle, free ZnPP was released at a constant rate of 20–30%/day. In addition, SMA–ZnPP micelle showed an apparent stoke's radius of 176.5 nm as measured by dynamic light scattering in a physiological solution [14]. It will further show a larger molecular size in circulation because of the albumin binding property of SMA [15,16]. Thus, the sustained in vivo antitumor effect was anticipated.

To investigate the therapeutic potential of SMA–ZnPP, in this study various tumor strains and normal cell lines were used to examine the pharmacological activity of SMA–ZnPP and the in vivo antitumor effect was evaluated by using various murine and rabbit tumor models. The intracellular uptake, pharmacokinetics and body distribution of SMA–ZnPP, and the safety were also investigated.

Table 1
IC_{50} of SMA–ZnPP against various tumor cells and normal cells.

Tumor cells	IC_{50} (μM)	Normal cells	IC_{50} (μM)
DLD-1	14.0	CV-1	50.0
Sk-Hep	16.0	HBE140	>50.0
HT-29	5.8	RLF	>200.0
A431	15.0	Hc	>50.0
KP-1N	3.6	HEK293	>50.0
CNE	19.4	CEF	25.2
ES2	9.8		
Lxc	4.2		
MCF-7	3.1		
Meth A	10.8		
B16/F10	20.1		
Mean	11.1 ± 1.9	Mean	>50.0

IC_{50} was determined by the MTT assay. See text for details.
DLD-1 and HT-29, human colon cancer cells; Sk-Hep, human liver cancer cell; A431, human lung cancer cell; CNE and Lxc, human laryngeal cancer cells; ES2, human ovarian cancer cell; KP-1N, human pancreatic cancer cell; MCF-7, human breast cancer cell; Meth A, mouse fibrosarcoma cell; B16/F10, mouse melanoma cell.
CV1, monkey kidney fibroblast; HBE140, human bronchial epithelial cell; RLF, rat liver fibroblast; HEK293, human embryonic kidney cell; CEF, chick embryonic fibroblast; Hc, human hepatic cell.

2. Materials and methods

2.1. Materials

Protoporphrin IX was purchased from Sigma-Aldrich (St. Louis, MO). SMA with a mean molecular size of 1280 Da (Mw/Mn: 1.1) was obtained from Kuraray Ltd., Kurashiki, Japan. Other reagents were of commercial reagent grade and were used without further purification.

2.2. Animals

Female BALB/c mice and male C57BL/6 mice, 5–6 weeks of age and weighing 20–25 g, as well as New Zealand white rabbits about 3 months old, weighing 2.0–2.25 Kg, were from SLC, Inc. (Shizuoka, Japan). All experiments were carried out according to the guidelines of the Laboratory Protocol of Animal Handling, Sojo University.

2.3. Synthesis of SMA–ZnPP micelles

The preparation, purification and characterization of SMA–ZnPP micelle were described in our recent work [14].

2.4. In vitro cytotoxicity assay

In vitro cytotoxicity of SMA–ZnPP micelles was examined by use of MTT assay with 11 tumor cell lines and six normal cell lines as described in Table 1. Cells were plated in 96-well culture plates (3000 cells/well). After overnight pre-incubation, predetermined concentration of SMA–ZnPP was added to respective culture media, and the cells were further incubated for 72 h. Toxicity was quantified as the fraction of surviving cells relative to untreated controls.

2.5. Intracellular uptake of SMA–ZnPP

Intracellular uptake study was carried out in human laryngeal cancer cells Lxc. 50,000 cells were cultured in 16-well plates. After 12 h of culture, SMA–ZnPP solution in deionized water or free ZnPP, dissolved first in DMSO and then diluted with 0.01 M NaOH, were added to the cells at dose of 5 μM ZnPP equivalent. The medium containing drug was removed at predetermined time, and the cells were washed twice with PBS. Cells were then lysed by 1 ml lysis buffer (4 N HCl in 70% ethanol) then heated to 70 °C for 15 min. The solution was centrifuged at 15,000 rpm for 3 min, and the supernatant was used for measuring the fluorescence emission from 550 to 600 nm by excitation at 420 nm (corresponding to ZnPP) using a fluorescence spectroscopy (Hitachi F-4500, Tokyo, Japan). Experiments were also carried out in mouse fibrosarcoma Meth A cells and mouse melanoma B16/F10 cells similarly.

2.6. Pharmacokinetics of SMA–ZnPP after i.v. injection into tumor-bearing mice

In vivo pharmacokinetics of SMA–ZnPP was examined by the use of ^{65}Zn-radiolabeled derivatives. Radiolabeled SMA–ZnPP was prepared by the same method as that described by Iyer et al [14], in which ^{65}Zn-labeled zinc acetate (Riken, Saitama, Japan) was used.

Mouse sarcoma S180 cells (2×10^6) were implanted, s.c. in the dorsal skin of ddY mice. At 10–15 days after tumor inoculation when tumors reached a diameter of 7–10 mm, each mouse received i.v. injections of ^{65}Zn-labeled SMA–ZnPP via the tail vein [50 μg ZnPP equivalent, 45,000 cpm (0.75 kBq), 0.2 ml/injection]. After scheduled time, mice were killed, blood samples were drawn from the inferior vena cava, and mice were then subjected to reperfusion with 20 ml of physiological saline containing heparin (5 units/ml) to remove blood components in the blood vessels of the tissues. Then, tumor tissues as well as normal tissues, including the liver, the spleen, the kidney, the intestine, the heart, the lung, the brain and the muscle, were collected and weighed. Radioactivity of these tissues was measured by using a gamma counter (1480 WIZARD, Perkin Elmer, Waltham, MA).

The pharmacokinetics of SMA–ZnPP was also examined in Meth A and B16 tumor-bearing mice as described below, by measuring the fluorescence intensity at 590 nm of ZnPP. Namely, at schedule time after SMA–ZnPP (20 mg/kg, ZnPP equivalent) i.v. injection, mice were killed and each tissue and organ was resected. Each tissue was then weighted, and dimethylsulfoxide was added at a ratio of 1 mL/100 mg tissue, followed by homogenization to extract the SMA–ZnPP by centrifugation (12,000 g, 25 °C, 10 min) to precipitate the insoluble tissue debris. Content of SMA–ZnPP in the supernatant was quantified by fluorescent intensity (Ex. 422 nm, Em. 590 nm).

2.7. In vivo antitumor effect of SMA–ZnPP

Mouse Meth A fibrosarcoma and melanoma B16 were prepared by implanting Meth A and B16/F10 cells (2×10^6 cells) s.c. in the dorsal skin of BALB/c and C57BL/6 mice, respectively. On day 7–10 after tumor injection when tumors had reached a diameter of 5–7 mm, SMA–ZnPP micelles at the desired concentration were administered intravenously via the tail vein according to the treatment protocol. Growth of the tumors was monitored every 2 days by measuring tumor volume with a digital caliper, which was estimated by measuring longitudinal cross section (L) and transverse section (W) according to the formula $V = (L \times W^2)/2$.

VX-2 carcinoma that is a papilloma virus-induced squamous cell carcinoma was established in New Zealand white rabbits. Briefly, laparotomy was performed with central incision, using pentobarbital sodium for general anesthesia at dose of 30 mg/kg intravenously. A solid VX-2 tumor mass of about $2 \times 2 \times 2$ mm^3 was inoculated through forceps into the subcapsular parenchyma of left anterior lobe of the liver. Fourteen days after tumor inoculation, intravenous treatment with SMA–ZnPP (once a week) was commenced for successive 4 weeks. One month after treatment, another laparotomy was performed and the liver was exposed to measure the diameter of tumor. Three months after tumor inoculation, all survived animals were sacrificed, and liver biopsy from the tumor site was collected for histological examination.

2.8. Histological examination

Tissue specimens collected from VX-2 tumor models as described above were fixed with 10% buffered neutral formalin solution and were then embedded in paraffin. Sections were stained with H&E as usual.

2.9. Measurement of HO activity

Meth A, B16 and S180 tumor tissues, collected from tumor-bearing mice after 24 h with or without i.v. injection of SMA–ZnPP (20 mg/kg, ZnPP equivalent), were homogenized by a Polytron homogenization with ice-cold homogenate buffer [20 mM potassium phosphate buffer (pH 7.4) plus 250 mM sucrose, 2 mM EDTA, 2 mM phenylmethylsulfonyl fluoride, and 10 μg/ml leupeptin]. Homogenates were centrifuged at 10,000g for 30 min at 4 °C, after which the resultant supernatant was ultracentrifuged at 105,000g for 1 h at 4 °C. The microsomal fraction was suspended in 0.1 M potassium phosphate buffer (pH 7.4) followed by sonication for 2 s at 4 °C. The reaction mixture used for measuring HO activity composed of microsomal protein (1 mg), cytosolic fraction of rat liver (1 mg of protein) as a source of biliverdin reductase, 33 μM hemin and 333 μM NADPH in 1 ml of 90 mM potassium phosphate buffer (pH 7.4). The mixture was incubated for 15 min at 37 °C, and then, the reaction was terminated by the addition of 33 μl of 0.01 M HCl. The bilirubin formed in the reaction was extracted with 1 ml of chloroform, and the bilirubin concentration was determined spectrophotometrically by measuring the difference in absorbance between 465 and 530 nm, with a molar extinction coefficient of 40 mM^{-1} cm^{-1}.

2.10. Safety of SMA–ZnPP micelles

BALB/c mice with Meth A tumors of about 5–7 mm in diameter were used for this study. SMA–ZnPP micelles were administered at the dose of 50 mg/kg (ZnPP equivalent), which is 5–10 times higher concentration than therapeutic dose. Seventy-two hours later, mice were killed and blood samples were obtained. RBC, WBC counts and hemoglobin levels were determined by using an automated blood counter (F-800 Microcell Counter, Toa Medical Electronics, Kobe, Japan). Plasma obtained by centrifugation was used for measurement of enzyme activities of alanine aminotransferase, aspartate aminotransferase, lactate dehydrogenase, blood urea nitrogen and total creatine values by using a sequential multiple Auto Analyzer system (Hitachi Ltd., Tokyo, Japan).

2.11. Statistical analyses

All data were expressed as means ± SD. Student's t-test was used to compare differences between experimental groups, and it was considered statistically significant when $p < 0.05$.

3. Results

3.1. In vitro cytotoxicity of SMA–ZnPP

In human liver cancer Sk-Hep cells, SMA–ZnPP exhibited remarkable cytotoxicity, in a dose-dependent manner, whereas

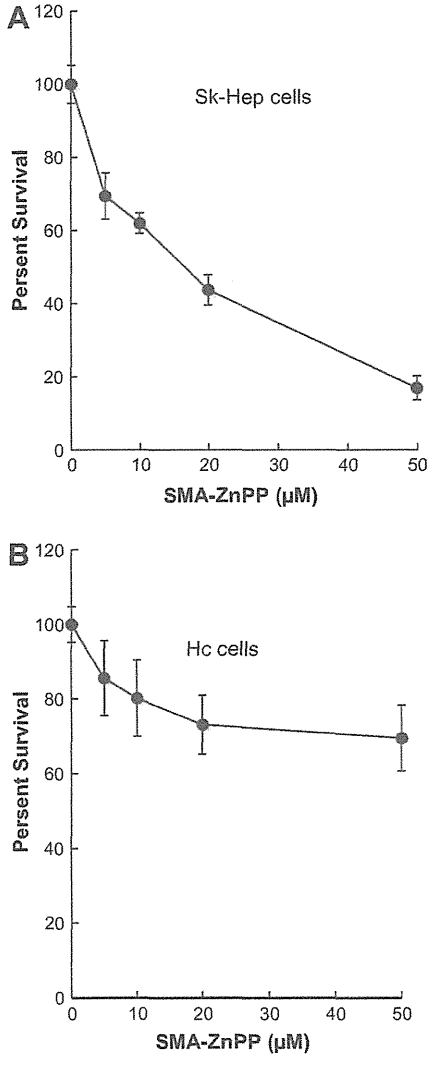

Fig. 1. In vitro cytotoxicity of SMA–ZnPP against normal (Hc) and tumor (Sk-Hep) cells. Cells were exposed to increasing concentration of SMA–ZnPP for 48 h, followed by MTT assay to determine cell viability. Values are mean ± SE (n = 6–8).

no significant cytotoxicity was observed up to 50 μM against normal hepatocytes Hc (Fig. 1 and Table 1). Similar results were found in other tumor and normal cell lines. The average 50% inhibitory concentration (IC_{50}) of SMA–ZnPP against different cells was summarized in Table 1. Most normal cells tested in this study exhibited relative tolerance to SMA–ZnPP treatment with IC_{50} of higher than 50 μM. In contrast, tumor cells showed much sensitive to this treatment, whose average IC_{50} was 11.1 ± 1.9 μM.

3.2. Intracellular uptake of SMA–ZnPP micelle

Fig. 2A shows a time-dependent internalization of SMA–ZnPP into Lxc cells, which is comparable to that of free ZnPP. These results suggest that the micellar formation of SMA did not impede the intracellular uptake of SMA–ZnPP. Instead, SMA–ZnPP appears more favorable than PEG–ZnPP micelles whose internalization was about 1/3 of that of SMA–ZnPP at 6 h after addition to the culture media (Fig. 2A). Similar results were obtained in Meth A (Fig. 2B) and B16/F10 cells (Fig 2C).

3.3. Pharmacokinetics and body distribution of SMA–ZnPP after i.v. injection

As shown in Fig. 3A, no significant prolonged plasma half-life ($t_{1/2}$) was observed for SMA–ZnPP. Namely, more than 50% of the SMA–ZnPP was removed from circulation during 10 min after i.v. injection. Moreover, no significant tumor accumulation of SMA–ZnPP was achieved, for example, the tumor concentration of SMA–ZnPP at 24 h after SMA–ZnPP administration was similar to those of most normal tissues (Fig. 3B).

However, surprisingly we found a remarkable increase in liver delivery of SMA–ZnPP, which is more than 20 times of that in plasma at 24 h after i.v. injection (Fig. 3A). Accumulation of SMA–ZnPP in liver tissue remained high for at least 4 days (Fig. 3A). Similar results were also observed in Meth A fibrosarcoma tumor and B16 melanoma tumor-bearing mice, respectively (Fig. S1). These findings suggested the potential application of SMA–ZnPP for cancers in the liver.

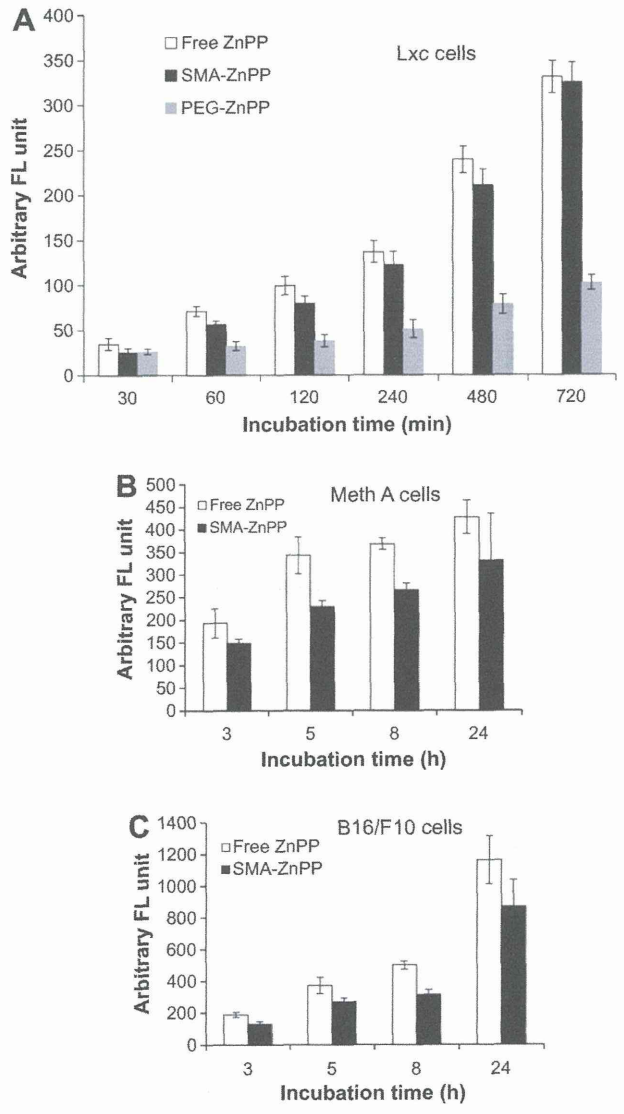

Fig. 2. Intracellular uptake of free ZnPP, SMA–ZnPP and PEG–ZnPP. Lxc cells (A), Meth A cells (B) and B16/F10 cells (C) were incubated with the investigated compounds at 5 μM (expressed in ZnPP equivalents) for different period of time. The amount of drug uptake by different tumor cells was determined measuring the fluorescence intensity after extracted from the cells, as described in Materials and Methods (2.5.). Values are mean ± SE (n = 4).

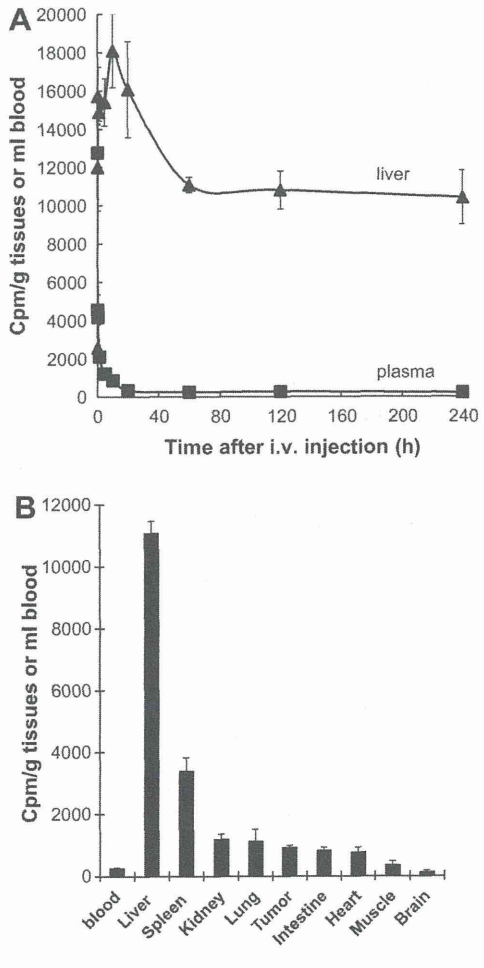

Fig. 3. Pharmacokinetics of SMA–ZnPP in ddY mice bearing Sarcoma 180 tumor as determined by using radioactive derivatives. Radiolabeled SMA–ZnPP was injected i.v. into tumor-bearing mice. After scheduled time periods, mice were killed, and samples of blood, tumor, liver and other normal tissues and organs were collected. Radioactivity of each tissue or organ was then measured. *A*, time-dependent change in SMA–ZnPP concentrations in plasma (■) and liver (▲). *B*, body distribution of SMA–ZnPP at 24 h after i.v. injection. Data are expressed as means; bars, ±SE (n = 4).

3.4. In vivo antitumor activity of SMA–ZnPP

Based on the findings of pharmacokinetics of SMA–ZnPP described in Fig. 3, we first investigated the in vivo antitumor effect of SMA–ZnPP in rabbit VX-2 tumor model transplanted in the liver. As shown in Fig. 4 and Table 2, a remarkable antitumor effect of SMA–ZnPP was observed. At 40 days after tumor transplantation, all of the non-drug treated control tumor-bearing rabbits died, whereas all animals receiving SMA–ZnPP did survive (Table 2). On days 60 and 80 after VX-2 tumor inoculation, when SMA–ZnPP was given at 4 and 8 mg/kg (ZnPP equivalent, weekly injection for 4 weeks), the survival rate was 60% and 80%, respectively, whereas 12 mg/kg resulted 100% survival on day 80 (Table 2). More important, histological examination showed that tumors became necrotic and fibrosis after SMA–ZnPP treatment (Fig. 4). In a long-term study, out of seven animals treated with 7 mg/kg weekly for 4 weeks, four animals were cured with no recurrence of the tumor of up to 2 years period of follow-up.

Further, the antitumor activity of SMA–ZnPP was examined in a Meth A mouse fibrosarcoma model. As shown in Fig. 5A, tumor growth was remarkably suppressed when SMA–ZnPP was administered at the dose of 4 mg/kg. Growth suppression continued to at least for 19 days after injection of SMA–ZnPP.

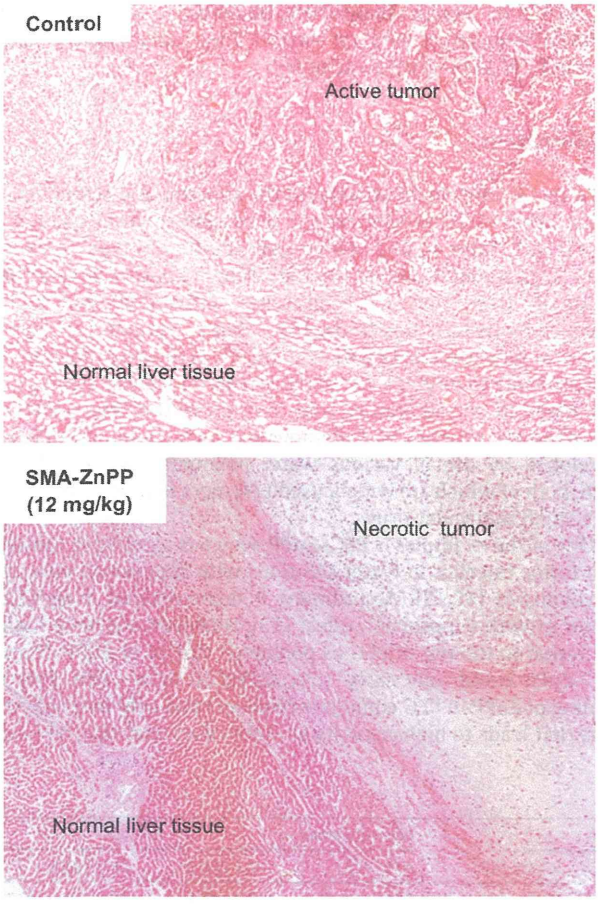

Fig. 4. Histological changes in rabbit VX-2 transplanted liver cancer after SMA–ZnPP treatment. Establishment of the tumor model is described in Materials and Methods. The dose of SMA–ZnPP was 12 mg/kg (ZnPP equivalent). Animals were killed, and tumor tissues were collected at 30 days (control group) and 60 days (SMA–ZnPP treatment group) after tumor inoculation, which were fixed by 10% buffered neutral formalin solution and were then subjected to H&E staining.

Table 2
Therapeutic effect of SMA–ZnPP on rabbit VX-2 papiloma implanted in the liver.

Group	Dose (mg/kg)[a]	% Survival after treatment[c]			Histological changes (by laparotomy)
		40 days[b]	60 days[b]	80 days[2]	
Control	0	0	0	0	Growing with invasion
SMA–ZnPP	4	100	60	60	Fibrosis appearing
	8	100	80	80	Necrosis, fibrosis in tumors
	12	100	100	100	Necrosis, totally fibrosis

See text and Fig. 4 for details.
[a] ZnPP equivalent. SMA–ZnPP was injected once weekly for 4 weeks at the indicated doses.
[b] Days after tumor inoculation.
[c] $n = 5–7$ Per group.

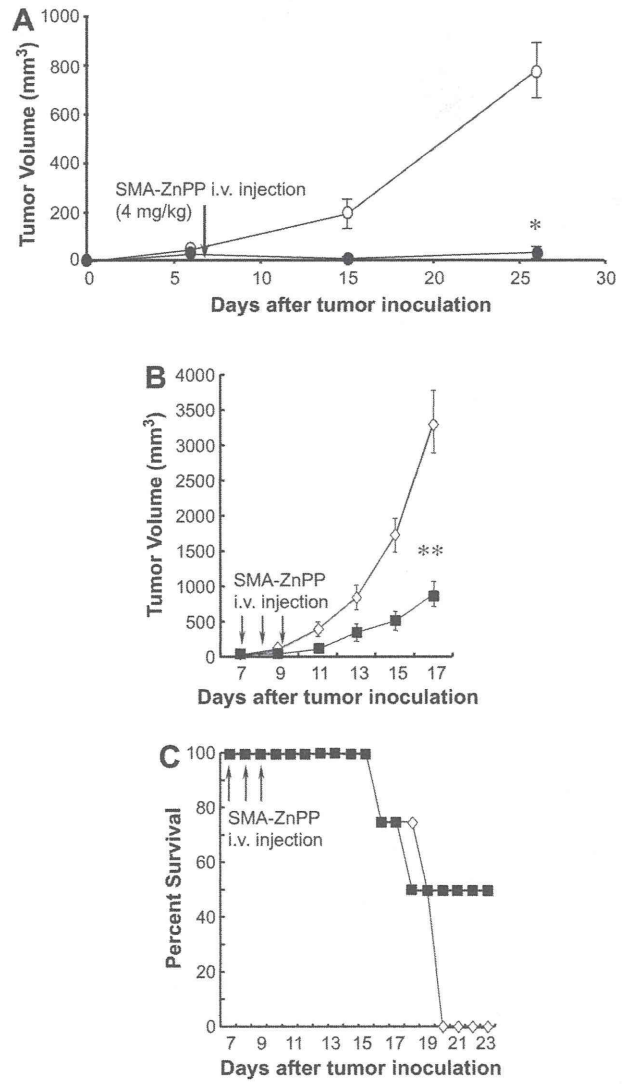

Fig. 5. *In vivo* antitumor effect of SMA–ZnPP. A shows the results in mouse MethA tumor model; ○, no drug control; ●, SMA–ZnPP (4 mg/kg ZnPP equivalent). B and C show the results of change in tumor size and survival of mouse B16 melanoma model; ◇, no drug control; ■, SMA–ZnPP (30 mg/kg ZnPP equivalent). Arrows indicate injections of SMA–ZnPP. Data are means ($n = 6–8$); bars, SE. $^{*}P < 0.0001$; $^{**}P < 0.001$, SMA–ZnPP treatment group vs untreated control group.

Similarly, in B16 melanoma in mice, which is known to progress rapidly and difficult to cure, significant suppression of tumor growth was found after 3 continuous injection of SMA–ZnPP at a

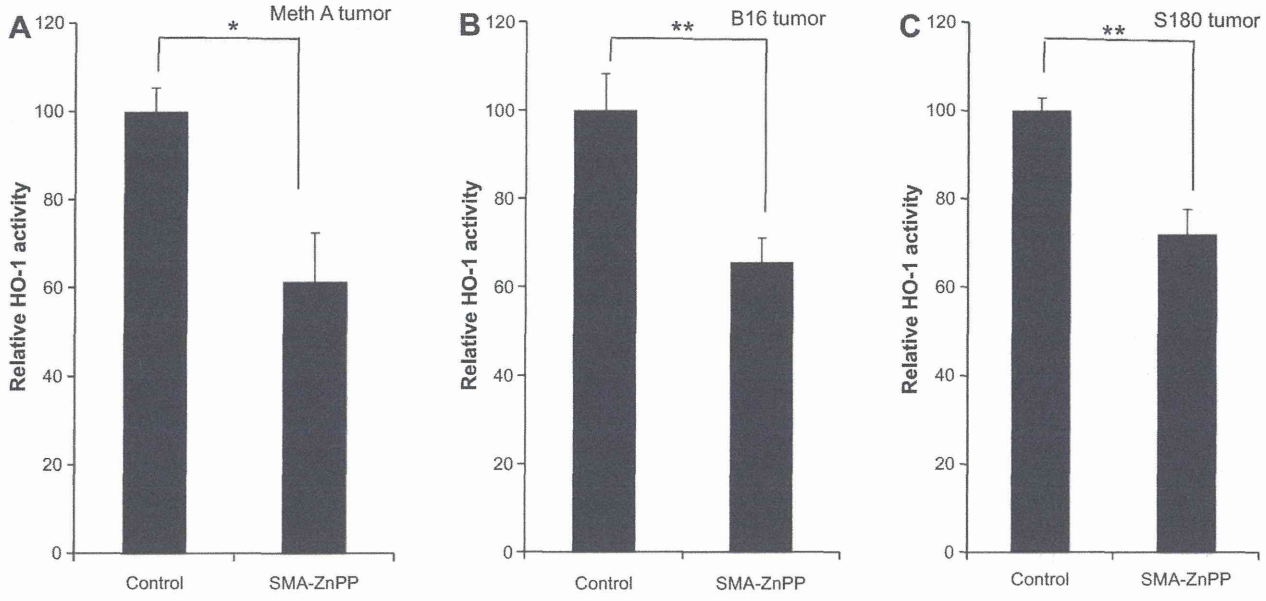

Fig. 6. Modulation by SMA–ZnPP of HO-1 activity in the Meth A (A), B16 (B) and S180 (C) solid tumor models. Tumor-bearing mice were i.v. injected with SMA–ZnPP (20 mg/kg, ZnPP equivalent). Twenty-four hours after the injection, tumors were obtained and were used for HO activity. Control mice values are means (n = 3–5); bars, SE. $^{*}P < 0.01$; $^{**}P < 0.005$, SMA–ZnPP treatment group vs untreated control group.

high dose (30 mg/kg) (Fig. 5B). Moreover, this treatment significantly contributed in the survival of tumor-bearing mice, that is, at 21 day after tumor inoculation, all mice of untreated control group died, whereas 50% of the mice in SMA–ZnPP treatment group remained alive (Fig. 5C).

3.5. Inhibition by SMA–ZnPP of HO activity in Meth A and B16 solid tumor

To clarify whether the in vivo suppression of tumor growth by SMA–ZnPP was due to the inhibition of HO activity, the enzyme activity of HO-1 in tumor after SMA–ZnPP treatment was examined. As shown in Fig. 6, HO-1 activity was significantly suppressed in all tested tumors (by 30–40%). These findings support our working hypothesis of the antitumor mechanisms of SMA–ZnPP, that is, through the HO-1 inhibition pathway, at least partly.

3.6. Adverse effect of SMA–ZnPP treatment

As summarized in Table 3, no significant adverse effects such as decreases in RBC and WBC counts and hemoglobin levels were found 72 h after SMA–ZnPP treatment at the dose of 50 mg/kg, which is much higher than the therapeutic dose or effective dose. Also, no significant changes in the liver enzymes and kidney functions were found under the same conditions (Table 3).

In addition, in a long-term follow-up of the above SMA–ZnPP treatment at high dose by a bolus administration (200 mg/kg), no death or body weight changes was observed up to 3 months after SMA–ZnPP injection (data not shown). These data strongly suggest the safety of SMA–ZnPP treatment.

4. Discussions

In this study, we demonstrated the superior and selective antitumor effect of SMA–ZnPP, both in vitro against various tumor cell lines (Fig. 1, Table 1), and in vivo against different type of solid tumors (Figs. 4 and 5), especially indicating its potential as a therapeutic for liver cancer. The antitumor activity of SMA–ZnPP is achieved by its targeting to the HO-1 that is a important "survival factor" of most tumors [2,5,6], which ZnPP is the pharmalogical active principle to inhibit HO-1 activity. This anticancer strategy was developed in our laboratory, and to improve the water-solubility and pharmacokinetics of ZnPP, micellar formations of ZnPP were developed by use of various water polymers, that is, PEG and SMA, both of which are widely used polymers to modify hardly soluble small molecular drugs.

One of the examples is PEG–ZnPP, which is a polymer conjugate that forms micelles in water solutions with superior in vivo pharmacokinetics [12,13]. Accordingly, it demonstrated a significant tumor growth suppression effect [13]. However, we have found a limitation to the use of PEG as polymeric carrier of ZnPP. Namely, PEG–ZnPP could only carry 1.5% ZnPP/PEG w/w ratio. This low loading of ZnPP in PEG conjugate requires relatively large injection dose that leads to high viscosity at higher dose that may be needed

Table 3
Effect of SMA–ZnPP in hematology and liver, kidney function.[a]

	Hematological findings			Kidney function		Liver enzymes		
	RBC (10^4/μl)	WBC (/μl)	Hb (g/l)	BUN (mg/dl)	Cr (mg/dl)	AST (IU/l)	ALT (IU/l)	LDH (IU/l)
Control	868.7 ± 60.6	186.7 ± 18.8	13.4 ± 1.2	23.0 ± 0.6	0.11 ± 0.01	395.3 ± 91.8	26.0 ± 3.8	10697.5 ± 2247.6
SMA–ZnPP[b]	820.0 ± 70.5	206.5 ± 52.0	2.3 ± 1.2	25.9 ± 1.1	0.13 ± 0.01	351.8 ± 88.9	27.5 ± 2.7	9755.0 ± 1570.8

Abbreviations used are: Hb, hemoglobin; BUN, blood urea nitrogen; Cr, creatinine; AST, aspartate aminotransferase; ALT, alanine aminotransferase; LDH, lactate dehydrogenase.

[a] No significant difference was found between SMA–ZnPP treatment group and control group in all selected indices. Values are presented as means ± SE.

[b] SMA–ZnPP was administered i.v. at 50 mg/kg (ZnPP equivalent). Assays were carried out at 72 h after SMA–ZnPP treatment.

for possible human therapeutic application. Further, the cost of expensive PEG for such low loading drug results in relatively high drug cost, which will become a social problem. To overcome these drawbacks, we further developed a micellar type of ZnPP using SMA, namely SMA–ZnPP, which can achieve higher loading of 15–45% w/w [14]. The high loading did not affect its solubility in this micelle; on the contrary, it resulted in solubility of up to 150 mg/ml, which can exceed the solubility required for therapeutic application.

In addition to the increased water-solubility, SMA–ZnPP also showed faster cellular uptake in all three different tumor cell lines tested, which is comparable to that of free ZnPP. Namely, it was about three times higher than PEG–ZnPP (Fig. 2). In our recent report, we compared the intracellular fate of free ZnPP and its polymer conjugates and micells (i.e., SMA–ZnPP and PEG–ZnPP) [17]. While free ZnPP was taken up via free diffusion, SMA–ZnPP was mostly internalized by endocytosis. During this internalization process, the micelle integrity was disrupted and free ZnPP appeared to be released upon internalization with cell membrane components [17]. However, the intracellular uptake of PEG–ZnPP was greatly impeded, which is called PEG dilemma [17,18]. The data in present study are consistent with our previous findings, suggesting that SMA–ZnPP shows stronger cytotoxicity than PEG–ZnPP because of its efficient cell uptake. To verify this notion, we tested the cytotoxicity of SMA–ZnPP in various tumor cells, which exhibited a mean IC_{50} of 11.1 μM (Table 1), whereas as reported previously, PEG–ZnPP showed a relatively higher IC_{50} of about 20 μM [13].

SMA–ZnPP micelle appeared as large molecule with the apparent molecular size of 144 kDa as determined by size exclusion chromatography [14]. As such large molecule, we thus anticipated its higher intratumor concentration based on the EPR effect followed by rapid endocytosis. It appears to be an universal phenomenon of macromolecular drugs with molecular weight larger than 40 kDa, a feature of the EPR effect, which they are selectively accumulated and being retained in solid tumor because of the unique anatomical and pathophysiological characteristics of tumor vasculature [19], and it is now known as a gold standard for the design and development of anticancer drugs [20–26].

However, we could not find good EPR effect for SMA–ZnPP in the present study, even tough it showed stable macromolecular micellar structure in physiological solution as described in our previous report [14]. This may be probably due to the lack of in vivo stability particularly in circulation, namely SMA–ZnPP micelle may be disrupted during circulation or upon uptake by RES which are rich in liver and spleen. Because of the high affinity to liver and spleen, free ZnPP released from SMA–ZnPP after disruption will accumulate mostly in liver and spleen. In consistent with this notion, we found interestingly that SMA–ZnPP significantly accumulated in liver tissue, for example, 20 times higher than plasma concentration at 24 h after i.v. injection, and it retained in the liver tissue at relatively high concentration for more than 96 h (Fig. 3C). The disruption and high liver accumulation of SMA–ZnPP could be improved by conjugation of SMA with ZnPP via a convalent amide bond (unpublished data). These data of distribution study, however, strongly suggest us to use SMA–ZnPP for the treatment of the liver cancer that is very difficult to treat in clinic with high mortality. Accordingly, in the present study, a significant cure rate of rabbits with VX-2 tumor implanted in the liver was achieved by using SMA–ZnPP, evidences being not only by the survival rate of animals, but also by the histopathological examination, that is, SMA–ZnPP treatment resulted in more necrosis as well as fibrosis of tumor tissues (Fig. 4 and Table 2).

Moreover, in other tumor models, that is, Meth A and B16 melanoma, SMA–ZnPP markedly reduced the tumor volume (Fig. 5), though complete regression of the tumor was not possible in B16 melanoma as in VX-2. In addition, compared to B16 tumors, Meth A tumors showed higher sensitivity to this treatment. Namely, a lower dose of SMA–ZnPP (at 4 mg/kg bolus i.v.) exhibited relatively remarkable tumor suppression effect (Fig. 5A) compared to B16 tumor with higher dose treatment of SMA–ZnPP (three injections of 30 mg/kg) (Fig. 5B). These findings are consistent with the cytotoxicity data of these two cell lines (IC_{50} of Meth A, 10.8 μM vs 20.1 μM of B16, Table 1).

The antitumor mechanisms of SMA–ZnPP were considered mostly due to the HO inhibition activity, and variation of HO-1 dependence susceptibility in different tumors may result in the variation of therapeutic effect. This notion was partly verified in the present study, namely, SMA–ZnPP treatment decreased the HO-1 activity in Meth A, B16 and S180 solid tumors, significantly though not largely (Fig. 6). It should be also noted that many other possible mechanisms may also work for the antitumor activity of SMA–ZnPP. For example, it has been reported that ZnPP-induced apoptosis of hamster fibroblasts by upregulating p53 expression, through ZnPP-mediated Egr-1 binding [27]. More recently, down-regulation of BCR/ABL oncogene by ZnPP in case of chronic myeloid leukemia (CML) has been reported [28]. Administration of PEG–ZnPP or SMA–ZnPP showed a remarkable therapeutic potential against CML [29,30], even imatinib-resistant CML [31]. In addition, SMA copolymer itself was found to have an active role in endogenous interferon induction as well as the activation of NK cells [32–34]. Furthermore, zinc is also known as an essential messenger molecule in stimulating immune response [35], and it was also used for the treatment of prostate cancer, probably via a mitochondrial-mediated apoptotic pathway [36–38]; it thus may serve as another mechanism of SMA–ZnPP-induced antitumor effect by releasing zinc from the porphyrin ring of ZnPP. The roles of various factors in mediating different anticancer activity of SMA–ZnPP in tumors, however, remain to be investigated.

Even though SMA–ZnPP accumulated predominantly in the liver tissues, we did not find apparent adverse effects during our experiments. In addition, no deterioration of the liver functions was observed even at high dose of SMA–ZnPP (50 mg/kg) (Table 3). This may be, at least partly, due to the differences of sensitivities to SMA–ZnPP between normal and tumor cells. This notion was supported by in vitro MTT assay, which showed a relatively strong cytotoxicity of SMA–ZnPP against various tumor cells (Table 1), that is, the IC_{50} of SMA–ZnPP to human liver cancer cells Sk-Hep was 16 μM, and the range of IC_{50} in different tumor cells was between 3 and 20 μM. Importantly and interestingly, normal cells seemed to be much tolerant to SMA–ZnPP. Namely, the IC_{50} of SMA–ZnPP to normal hepatocytes Hc was higher than 50 μM, as well as other normal cells (Table 1). The difference of the responses of tumor cells and normal cells against SMA–ZnPP treatment may be due to the difference of HO-1 expression between tumor and normal cells, as described earlier [2,5,6,13]; however, further investigations are needed to define this correlation.

SMA–ZnPP used in our animal study, with some exceptions, was at the dose range of 1–10 mg/kg; however, animals were able to tolerate as high as 50 mg/kg without any apparent toxicity as reflected by blood cells count and biochemical examination of liver and kidney functions (Table 3), as well as survival rate. These data indicate the high safety of SMA–ZnPP with a wide therapeutic window.

5. Conclusions

The water-soluble micellar type of HO-1 inhibitor SMA–ZnPP was found to be effective in many solid tumor models, especially VX-2 tumor transplanted in the liver of rabbit. The drug accumulated in the liver was very high, while clearance from the circula-

tion was relatively rapid. SMA–ZnPP was examined both in vitro and in vivo; whereas it showed relatively potent cytotoxicity to tumor cells (average IC_{50} of about 11 μM); the IC_{50} of normal cells was higher than 50 μM, which resulted in very little adverse effects to tumor-bearing animals. These findings suggest the potential use of SMA–ZnPP as a novel anticancer drug especially for liver cancer, which warrants further development and investigation.

Acknowledgment

The authors wish to thank Dr. Takahiro Seki for excellent technical assistance.

Appendix A. Supplementary material

Supplementary data associated with this article can be found, in the online version, at http://dx.doi.org/10.1016/j.ejpb.2012.04.016.

References

[1] M.D. Maines, Heme oxygenase: function, multiplicity, regulatory mechanisms, and clinical applications, FASEB J. 2 (1988) 2257–2268.
[2] J. Fang, T. Akaike, H. Maeda, Antiapoptotic role of heme oxygenase (HO) and the potential of HO as a target in anticancer treatment, Apoptosis 9 (2004) 27–35.
[3] S.M. Keyse, R.M. Tyrrell, Heme oxygenase is the major 32-kDa stress protein induced in human skin fibroblasts by UVA radiation, hydrogen peroxide, and sodium arsenite, Proc. Natl. Acad. Aci. USA 86 (1989) 99–103.
[4] R. Motterlini, R. Foresti, R. Bassi, B. Calabrese, J.E. Clark, C.J. Green, Endothelial heme oxygenase-1 induction by hypoxia. Modulation by inducible nitric oxide synthase and S-nitrosothiols, J. Biol. Chem. 275 (2000) 13613–13620.
[5] K. Doi, T. Akaike, S. Fujii, S. Tanaka, N. Ikebe, T. Beppu, S. Shibahara, M. Ogawa, H. Maeda, Induction of haem oxygenase-1 by nitric oxide and ischaemia in experimental solid tumours and implications for tumour growth, Br. J. Cancer 80 (1999) 1945–1954.
[6] S. Tanaka, T. Akaike, J. Fang, T. Beppu, M. Ogawa, F. Tamura, Y. Miyamoto, H. Maeda, Antiapoptotic effect of haem oxygenase-1 induced by nitric oxide in experimental solid tumour, Br. J. Cancer 88 (2003) 902–909.
[7] J.P. Greenstein, Biochemistry of Cancer, second ed., Academic Press, New York, 1954.
[8] Y. Hasegawa, T. Takano, A. Miyauchi, F. Matsuzaka, H. Yoshida, K. Kuma, N. Amino, Decreased expression of glutathione peroxidase mRNA in thyroid anaplastic carcinoma, Cancer Lett. 182 (2002) 69–74.
[9] N. Yamanaka, D. Deamer, Superoxide dismutase activity in WI-38 cell cultures: effect of age, trypsinization and SV-40 transformation, Physiol. Chem. Phus. 6 (1974) 95–106.
[10] K. Sato, K. Ito, H. Kohara, Y. Yamaguchi, K. Adachi, H. Endo, Negative regulation of catalase gene expression in hepatoma cells, Mol. Cell. Biol. 12 (1992) 2525–2533.
[11] J. Fang, D. Deng, H. Nakamura, T. Akuta, H. Qin, A.K. Iyer, K. Greish, H. Maeda, Oxystress inducing antitumor therapeutics via tumor-targeted delivery of PEG-conjugated D-amino acid oxidase, Int. J. Cancer 122 (2008) 1135–1144.
[12] S.K. Sahoo, T. Sawa, J. Fang, S. Tanaka, Y. Miyamoto, T. Akaike, H. Maeda, Pegylated zinc protoporphyrin: a water-soluble heme oxygenase inhibitor with tumor-targeting capacity, Bioconjug. Chem. 13 (2002) 1031–1038.
[13] J. Fang, T. Sawa, T. Akaike, T. Akuta, S.K. Sahoo, G. Khaled, A. Hamada, H. Maeda, In vivo antitumor activity of pegylated zinc protoporphyrin: targeted inhibition of heme oxygenase in solid tumor, Cancer Res. 63 (2003) 3567–3574.
[14] A.K. Iyer, K. Greish, J. Fang, R. Murakami, H. Maeda, High-loading nanosized micelles of copoly(styrene-maleic acid)–zinc protoporphyrin for targeted delivery of a potent heme oxygenase inhibitor, Biomaterials 28 (2007) 1871–1881.
[15] A. Kobayashi, T. Oda, H. Maeda, Protein binding of macromolecular anticancer agent SMANCS: characterization of poly(styrene-co-maleic acid) derivatives as an albumin binding ligand, J. Bioact. Compat. Polym. 3 (1988) 319–333.
[16] K. Greish, A. Nagamitsu, J. Fang, H. Maeda, Copoly(styrene-maleic acid)–pirarubicin micelles: high tumor-targeting efficiency with little toxicity, Bioconjug. Chem. 16 (2005) 230–236.
[17] H. Nakamura, J. Fang, B. Gahininath, K. Tsukigawa, H. Maeda, Intracellular uptake and behavior of two types zinc protoporphyrin (ZnPP) micelles, SMA–ZnPP and PEG–ZnPP as anticancer agents; unique intracellular disintegration of SMA micelles, J. Control. Release 155 (2011) 367–375.
[18] H. Hatakeyama, H. Akita, H. Harashima, A multifunctional envelope type nano device (MEND) for gene delivery to tumours based on the EPR effect: a strategy for overcoming the PEG dilemma, Adv. Drug Deliv. Rev. 63 (2011) 152–160.
[19] Y. Matsumura, H. Maeda, A new concept for macromolecular therapeutics in cancer chemotherapy: mechanism of tumoritropic accumulation of proteins and the antitumor agent SMANCS, Cancer Res. 46 (1986) 6387–6392.
[20] H. Maeda, T. Sawa, T. Konno, Mechanism of tumor-targeted delivery of macromolecular drugs, including the EPR effect in solid tumor and clinical overview of the prototype polymeric drug SMANCS, J. Control. Release 74 (2001) 47–61.
[21] K. Greish, J. Fang, T. Inutsuka, A. Nagamitsu, H. Maeda, Macromolecular therapeutics: advantages and prospects with special emphasis on solid tumour targeting, Clin. Pharmacokinet. 42 (2003) 1089–1105.
[22] H. Maeda, Tumor-selective delivery of macromolecular drugs via the EPR effect: background and future prospects, Bioconjug. Chem. 21 (2010) 797–802.
[23] R. Duncan, The dawning era of polymer therapeutics, Nat. Rev. Drug Discov. 2 (2003) 347–360.
[24] H. Maeda, G.Y. Bharate, J. Daruwalla, Polymeric drugs for efficient tumor-targeted drug delivery based on EPR-effect, Eur. J. Pharm. Biopharm. 71 (2009) 409–419.
[25] T. Seki, J. Fang, H. Maeda, Tumor targeted macromolecular drug delivery based on the enhanced permeability and retention effect in solid tumor, in: Y. Lu, R.I. Mahato (Eds.), Pharmaceutical Perspectives of Cancer Therapeutics, AAPS-Springer Publishing, New York, 2009, pp. 93–102.
[26] J. Fang, H. Nakamura, H. Maeda, The EPR effect: unique features of tumor blood vessels for drug delivery, factors involved, and limitations and augmentation of the effect, Adv. Drug Deliv. Rev. 63 (2010) 136–151.
[27] G. Yang, X. Nguyen, J. Qu, P. Rekulapelli, D.K. Stevenson, P.A. Dennery, Unique effects of zinc protoporphyrin on HO-1 induction and apoptosis, Blood 97 (2001) 1306–1313.
[28] M. Mayerhofer, S. Florian, M.T. Krauth, K.J. Aichberger, M. Bilban, R. Marculescu, D. Printz, G. Fritsch, O. Wagner, E. Selzer, W.R. Sperr, P. Valent, C. Sillaber, Identification of heme oxygenase-1 as a novel BCR/ABL-dependent survival factor in chronic myeloid leukemia, Cancer Res. 64 (2004) 3148–3154.
[29] R. Kondo, K.V. Gleixner, M. Mayerhofer, A. Vales, A. Gruze, P. Samorapoompichit, K. Greish, M.T. Krauth, K.J. Aichberger, W.F. Pickl, H. Esterbauer, C. Sillaber, H. Maeda, P. Valent, Identification of heat shock protein 32 (Hsp32) as a novel survival factor and therapeutic target in neoplastic mast cells, Blood 110 (2007) 661–669.
[30] E. Hadzijusufovic, L. Rebuzzi, K.V. Gleixner, V. Ferenc, B. Peter, R. Kondo, A. Gruze, M. Kneidinger, M.T. Krauth, M. Mayerhofer, P. Samorapoompichit, K. Greish, A.K. Iyer, W.F. Pickl, H. Maeda, M. Willmann, P. Valent, Targeting of heat-shock protein 32/heme oxygenase-1 in canine mastocytoma cells is associated with reduced growth and induction of apoptosis, Exp. Hematol. 36 (2008) 1461–1470.
[31] M. Mayerhofer, K.V. Gleixner, J. Mayerhofer, G. Hoermann, E. Jaeger, K.J. Aichberger, R.G. Ott, K. Greish, H. Nakamura, S. Derdak, P. Samorapoompichit, W.F. Pickl, V. Sexl, H. Esterbauer, I. Schwarzinger, C. Sillaber, H. Maeda, P. Valent, Targeting of heat shock protein 32 (Hsp32)/heme oxygenase-1 (HO-1) in leukemic cells in chronic myeloid leukemia: a novel approach to overcome resistance against imatinib, Blood 111 (2008) 2200–2210.
[32] F. Suzuki, R.B. Pollard, S. Uchimura, T. Munakata, H. Maeda, Role of natural killer cells and macrophages in the nonspecific resistance to tumors in mice stimulated with SMANCS, a polymer-conjugated derivative of neocarzinostatin, Cancer Res. 50 (1990) 3897–3904.
[33] F. Suzuki, T. Munakata, H. Maeda, Interferon induction by SMANCS: a polymer-conjugated derivative of neocarzinostatin, Anticancer Res. 8 (1988) 97–103.
[34] T. Oda, T. Morinaga, H. Maeda, Stimulation of macrophage by polyanions and its conjugated proteins and effect on cell membrane, Proc. Soc. Exp. Biol. Med. 181 (1986) 9–17.
[35] H. Haase, J.L. Ober-Blöbaum, G. Engelhardt, S. Hebel, A. Heit, H. Heine, L. Rink, Zinc signals are essential for lipopolysaccharide-induced signal transduction in monocytes, J. Immunol. 181 (2008) 6491–6502.
[36] L.C. Costello, R.B. Franklin, P. Feng, Mitochondrial function, zinc, and intermediary metabolism relationships in normal prostate and prostate cancer, Mitochondrion 5 (2005) 143–153.
[37] P. Feng, T. Li, Z. Guan, R.B. Franklin, L.C. Costello, The involvement of Bax in zinc-induced mitochondrial apoptogenesis in malignant prostate cells, Mol. Cancer 7 (2008) 25.
[38] S.F. Lin, H. Wei, D. Maeder, R.B. Franklin, P. Feng, Profiling of zinc-altered gene expression in human prostate normal vs. cancer cells: a time course study, J. Nutr. Biochem. 20 (2009) 1000–1012.

Original Research

PEGylated D-amino acid oxidase restores bactericidal activity of neutrophils in chronic granulomatous disease via hypochlorite

Hideaki Nakamura[1,2], Jun Fang[1,2], Tomoyuki Mizukami[3], Hiroyuki Nunoi[4] and Hiroshi Maeda[2]

[1]Laboratory of Microbiology and Oncology, Faculty of Pharmaceutical Science; [2]Institute for Drug Delivery System Research, Sojo University, Ikeda 4-22-1, Kumamoto 860-0082; [3]Department of Pediatrics, Kumamoto Saishunsou National Hospital, 2659 Suya, Kohshi, Kumamoto 861-1196; [4]Division of Pediatrics, Department of Reproductive and Developmental Medicine, Faculty of Medicine, University of Miyazaki, Kiyotake-cho, Kihara 5200, Miyazaki 889-1692, Japan
Corresponding author: Hiroshi Maeda. Email: hirmaeda@ph.sojo-u.ac.jp

Abstract

Chronic granulomatous disease (CGD) causes impaired hydrogen peroxide (H_2O_2) generation. Consequently, neutrophils in patients with CGD fail to kill infecting pathogens. We expected that supplementation with H_2O_2 would effectively restore the bactericidal function of neutrophils in CGD. Here, we used polyethylene glycol-conjugated D-amino acid oxidase (PEG-DAO) as an H_2O_2 source. The enzyme DAO generates H_2O_2 by using D-amino acid and oxygen as substrates. PEG-DAO plus D-amino acid indeed exerted bacteriostatic activity against *Staphylococcus aureus* via H_2O_2 *in vitro*. Furthermore, use of PEG-DAO plus D-amino acids, which increased the amount of intracellular H_2O_2, restored bactericidal activity of neutrophils treated with diphenylene iodonium, in which nicotinamide adenine dinucleotide phosphate (NADPH) oxidase was defective. This restoration of bactericidal activity was mediated by myeloperoxidase, with concomitant production of H_2O_2 by PEG-DAO plus D-Ala. We also confirmed that PEG-DAO treatment restored bactericidal activity of congenitally defective neutrophils from patients with CGD. These results indicate that PEG-DAO can supply additional H_2O_2 for defective NADPH oxidase of neutrophils from patients with CGD, and thus neutrophils regain bactericidal activity.

Keywords: PEG-DAO, chronic granulomatous disease, hydrogen peroxide, H_2O_2 supplementation therapy

Experimental Biology and Medicine 2012; **237**: 703–708. DOI: 10.1258/ebm.2012.011360

Introduction

Chronic granulomatous disease (CGD) is a genetic disorder characterized by chronic and recurrent pyogenic infections. Patients with CGD have a defect in nicotinamide adenine dinucleotide phosphate (NADPH) oxidase that results in dysfunctional production of hydrogen peroxide (H_2O_2).[1,2] H_2O_2 plays a pivotal role in the antibacterial function of neutrophils, mediated by myeloperoxidase (MPO), so the impaired H_2O_2 production means failure of bactericidal activity against pathogenic organisms such as *Staphylococcus aureus*.[2,3]

D-Amino acid oxidase (DAO) is an enzyme containing flavin adenine dinucleotide (FAD).[4] The biochemical function of DAO involves oxidative deamination of D-amino acids, which yields the corresponding α-keto acids, a process in which molecular oxygen is used as an electron acceptor and H_2O_2 is generated.[5]

We previously prepared polyethylene glycol (PEG)-conjugated DAO (PEG-DAO) with comparable enzyme activity to native DAO.[6,7] More importantly, PEG-DAO had a longer circulation time in the blood, and preferential accumulation in inflamed sites, as a result of the enhanced permeability and retention (EPR) effect.[8,9] Our previous report showed that PEG-DAO exhibited selective cytotoxicity against various cancer cells via production of H_2O_2 *in vivo* and *in vitro*.[6,7]

We therefore anticipated that PEG-DAO would function as an alternative supplier of H_2O_2 for neutrophils in patients with CGD. In this study, we therefore investigated the effect of PEG-DAO on bactericidal activity of neutrophils from mice in which NADPH oxidase was inhibited, and from a patient with CGD, and analyzed the mechanism of bactericidal activity, in addition to investigating MPO-inhibited neutrophils.

Materials and methods

Materials

S. aureus strain ATCC25923 was used in these studies. ICR mice were purchased from Japan SLC, Inc., Shizuoka,

Japan. Trypticase soy (SCD) broth was purchased from Nissui Seiyaku Co., Tokyo, Japan. Flavin adenine dinucleotide was purchased from Sigma-Aldrich Chemical Co. (St Louis, MO, USA). Trypticase soy agar, isopropyl-β-D-thiogalactopyranoside, carbenicillin, Tween-20, ammonium sulfate, casein sodium salt and other reagents were from Wako Pure Chemical Industries, Ltd, Osaka, Japan. 4-aminobenzoic acid hydrazide (4-ABH) was from Merck KGaA, Frankfurt, Germany. Diphenylene iodonium (DPI) was purchased from Tokyo Chemical Industry Co., Ltd, Tokyo, Japan. Succinimide-activated PEG (MEC-50HS), with an average molecular size of Mr 5000, was purchased from Nippon Oil & Fat Co. (Tokyo, Japan).

Preparation of PEG-DAO

Recombinant porcine DAO was prepared as described previously.[7] Briefly, *Escherichia coli* BL21 (DE3) bacteria harboring the pET3c plasmid encoding porcine DAO were cultured in LB medium containing 50 μg/mL carbenicillin, and porcine DAO expression was achieved by adding 10 μmol/L isopropyl-β-D-thiogalactopyranoside to the medium with *E. coli*. After culture of the bacteria at 37°C for 20 h, bacterial pellets were sonicated (150 W, 30 min) in 17 mmol/L pyrophosphate buffer (pH 8.2), and porcine DAO was obtained by heat denaturation at 59°C for three minutes, followed by ammonium sulfate precipitation at 35% saturation, and then diethylaminoethyl cellulose column chromatography ($L = 10$ cm $\times$ $\phi = 1.6$ cm). The purity of DAO (>90%) was determined by using sodium dodecylsulfate polyacrylamide gel electrophoresis after staining with Coomassie brilliant blue. PEGylation of DAO was conducted as described previously.[6] In brief, to the DAO solution (2.0 mg/mL protein in 50 mmol/L sodium phosphate buffer, pH 7.4), succinimide-activated PEG was added at a 3.5 mol/L excess of PEG/mol of free amino groups in DAO and was allowed to react for one hour at 4°C. The reaction mixture containing PEG-DAO thus obtained was then purified to remove free PEG and other low-molecular-weight reactants by ultrafiltration with the YM-10 membrane (Millipore) using 10 times the volume of 10 mmol/L phosphate-buffered saline (PBS). PEG-DAO was stored in PBS containing 0.1 mmol/L FAD at 4°C. Approximately 30% of the amino groups on DAO was reacted with PEG.

Bacteriostatic assay

S. aureus bacteria were cultured until the mid-log phase of growth in SCD broth with reciprocal shaking at 37°C. *S. aureus* were washed twice in saline and 1×10^6 CFU/mL of *S. aureus* were incubated with various concentrations of PEG-DAO, D-Ala, and with or without catalase in SCD broth at 37°C for five hours. The relative total numbers of bacteria were measured at turbidity at 570 nm and were correlated with the numbers of viable bacteria.

Preparation of neutrophils

Peritoneal neutrophils were elicited in 10-week-old female ICR mice by intraperitoneal injection of 3 mL per mouse of 6% casein sodium salt dissolved in physiological saline. At six hours after injection, neutrophils were harvested via peritoneal lavage with 5 mL of PBS, pH 7.4. Contaminating erythrocytes were removed by incubating in hypotonic saline solution (0.2% NaCl) for 30 s to cause erythrocytes to burst, after which isotonicity was restored via a rebalancing solution (1.9% NaCl) followed by centrifugation. Approximately 1×10^7 neutrophils were obtained from 10-week-old female ICR mice. The purity of the neutrophils (>90%) was checked by using Giemsa staining and examination of cell morphology with a conventional microscope (ECLIPSE TS100; Nikon, Tokyo, Japan). Human peripheral neutrophils were collected from a patient with CGD and a healthy volunteer using Polymorphprep™ (Cosmo Bio, Tokyo, Japan) according to the manufacturer's instruction. Briefly, 5 mL of human blood sample was carefully layered on the top of 5 mL of Polymorphprep™, followed by centrifugation with a swing-out rotor for 30 min at $450 \times g$. The neutrophil fraction was collected and mixed with 0.45% NaCl, and then centrifuged for 10 min at $400 \times g$. Neutrophil pellets were then resuspended in PBS (−) and used for further experiments.

Bactericidal activity of neutrophils and preparation of CGD neutrophil mimics

Mouse peritoneal neutrophils were preincubated with 10 DPI or 10 μmol/L 4-ABH at 37°C for 15 min. *S. aureus*, which were cultured in SCD broth until the mid-log phase growth, were treated with 10% pooled mouse serum for effective neutrophilic endocytosis of *S. aureus*. Bacteria were added to neutrophils at the bacteria-to-neutrophil ratio of 10:1 (1×10^6 neutrophils/mL), and incubation proceeded at 37°C with reciprocal shaking at 0.5 Hz. After 30 min of incubation, non-phagocytosed bacteria were removed by swing-out centrifugation (at $110 \times g$, 4 min) and neutrophils were washed three times with PBS (+) containing 10 μmol/L DPI. Phagocytosed bacteria were precipitated with neutrophils, but non-phagocytosed bacteria were retained in the supernatant. Neutrophils that ingested the bacteria were incubated at 37°C for 30 min with shaking, with increasing concentrations of PEG-DAO (10, 50 and 100 mU/mL) in the presence of 10 mmol/L D-Ala and PBS (+) containing 10 μmol/L DPI. Samples were diluted with 0.2% Tween-20, incubated at room temperature for five minutes to release phagocytosed bacteria, and vortexed vigorously, after which duplicate 100-μL aliquots were plated on 15 mL plates of SCD agar gel followed by overnight culture at 37°C. The numbers of viable bacteria were counted as described above.

Results

Bacteriostatic activity of PEG-DAO

We first examined the bacteriostatic activity of PEG-DAO against *S. aureus*. In the presence of 10 mmol/L D-Ala,

PEG-DAO showed bacteriostatic activity in a dose-dependent manner (Figure 1a). Different concentrations of D-Ala also demonstrated dose-dependent activity (Figure 1b). Bacteriostatic activity was not observed with treatment of PEG-DAO and L-Ala (Figure 1a). Adding 1 mg/mL catalase (5000–15,000 U/mL) to samples with PEG-DAO and D-Ala nullified the bacteriostatic activity of PEG-DAO (Figure 1c).

PEG-DAO restored antibacterial activity of NADPH oxidase-deficient mouse neutrophils

As H_2O_2 is a highly cell permeable oxidant, we examined H_2O_2 generated by PEG-DAO plus D-Ala in the medium to determine whether H_2O_2 could penetrate cell membranes and enter the cells. H_2O_2 treatment increased oxidative stress inside neutrophils, as shown by analysis using fluorescence flow cytometry in the presence of the fluorescent reactive oxygen species probe dichlorofluorescein diacetate (DCFH-DA) (Figure 2a). In the presence of 10 mmol/L D-Ala, treatment with PEG-DAO increased the intracellular H_2O_2 concentration in a dose-dependent manner as judged by this fluorescent probe (Figures 2b and c). However, PEG-DAO alone did not induce oxidative stress (data not shown). To mimic defective CGD neutrophils, mouse peritoneal neutrophils were treated with 10 μmol/L DPI to inhibit NADPH oxidase. DPI treatment increased the numbers of viable bacteria inside the treated neutrophils, as seen by the colony forming assay (Figure 2d). However, PEG-DAO treatment in the presence of 10 mmol/L D-Ala restored bactericidal activity of DPI-treated defective neutrophils; the number of viable bacteria inside neutrophils almost recovered to the normal, non-CGD control. No enhancement of antibacterial activity by PEG-DAO in normal neutrophils was observed (Figure 2d).

PEG-DAO induced MPO-dependent bactericidal activity of CGD-equivalent mouse neutrophils

Consistent with the results shown in Figure 2, the bactericidal activity of mouse peritoneal neutrophils, which had been pretreated with DPI and thus had no NADPH oxidase activity, was restored by adding PEG-DAO and D-Ala (Figure 3). Treatment with 4-ABH, a specific inhibitor of MPO, clearly suppressed the bactericidal activity of normal mouse neutrophils. An interesting finding was the significant suppression of bactericidal activity of neutrophils by 4-ABH treatment, even with added PEG-DAO and D-Ala. This result demonstrates the important role of MPO in PEG-DAO-mediated bacterial killing (Figure 3).

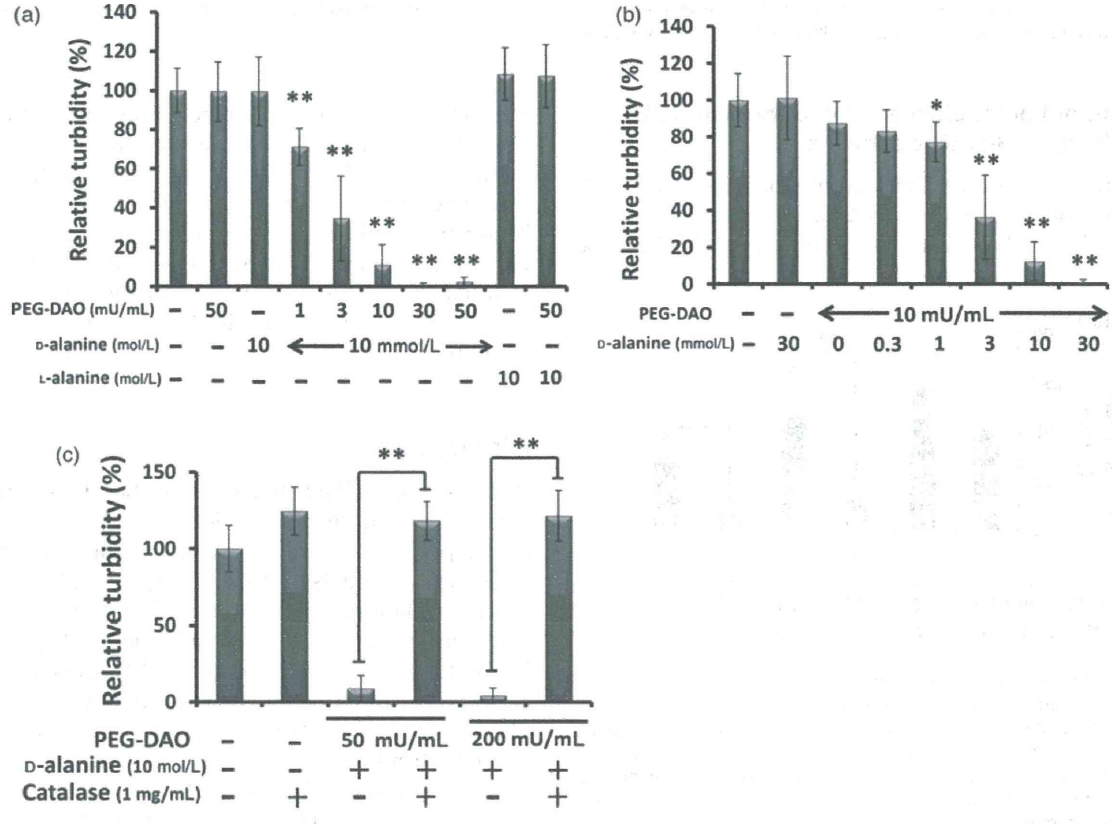

Figure 1 Bacteriostatic activity of polyethylene glycol-conjugated D-amino acid oxidase (PEG-DAO) against *Staphylococcus aureus*. (a) Increasing concentrations of PEG-DAO in the presence of 10 mmol/L D-Ala or (b) increasing concentrations of D-Ala in the presence of 10 mU/mL PEG-DAO were incubated with *S. aureus* bacteria (1×10^6 CFU/mL) for five hours, after which turbidity at 570 nm was measured. (c) *S. aureus* bacteria (1×10^6 CFU/mL) were incubated for five hours with PEG-DAO plus D-Ala with or without 1 mg/mL bovine catalase, and after which turbidity at 570 nm was measured. ** and * indicate statistically significant differences ($P < 0.01$) and ($P < 0.05$), respectively, by Student's *t*-test. Values are means ± SD ($n = 12$)